J Mater Sci (2008) 43:6902–6911
DOI 10.1007/s10853-008-2993-3

An important factor for controlling the photoreactivity of titania: O-deficiency of anatase thin films

Hiroki Nagai · Moyu Hasegawa · Hiroki Hara · Chihiro Mochizuki · Ichiro Takano · Mitsunobu Sato

Received: 22 May 2008 / Accepted: 4 September 2008 / Published online: 27 September 2008

Abstract Oxygen deficient (O-deficient) anatase thin films with high photoreactivity under UV-light irradiation were fabricated by post-annealing partially nitrided anatase thin films, prepared by heat-treatment of precursor films involving a Ti complex of EDTA on an FTO glass substrate at 500 °C for 30 min in an Ar gas flow, in air at 500 °C for 5–30 min. The anatase structure of the transparent thin films was characterized by using XRD and Raman spectra. The O/Ti peak area ratio determined by using XPS of the anatase film having the highest photoreactivity, which was evaluated according to the decoloration rate of methylene blue in an aqueous solution, was 1.5. The photoreactivity of the film was 2.1 times higher than that prepared by using the sol–gel method, with an O/Ti ratio of 1.7. The thin film with the highest photoreactivity indicated the smallest refractive index, 1.99.

Introduction

Anatase, one of the three crystal forms of titania, is an attractive material as a photoreactive semiconductor that can work under ultraviolet (UV) light irradiation. The photoreactivity of anatase depends upon the chemical reactivity of the electrons and holes photo-induced in the anatase particles. Fujishima et al. reported that the electrons and holes on the surface of anatase particles recombine immediately unless redox reactions do not occur with reactants such as O_2 and H_2O near the anatase surface [1]. Porous and fine anatase particles with larger specific surface areas are more effective to photoreactions, because the number of opportunities for reactions between photo-induced electrons and holes with reactants before their recombination increases [2, 3].

The fabrication of visible-light-responsive films with enhanced UV-sensitivity was achieved in our recent study [4]. Layer-structured anatase films were prepared by using a molecular precursor method, which employs coating solutions including the alkylammonium salts of anionic Ti complex of EDTA and OX ligands in an Ar gas flow, where EDTA and OX represent ethylenediamine-*N*,*N*,*N*′,*N*′-tetraacetic acid and oxalic acid, respectively. During heat-treatment of the precursor films in the Ar gas flow, transparent anatase thin films with enhanced UV-sensitivity and even surfaces were fabricated, although the UV-sensitivities of other visible-light-responsive thin films modified by impregnating metal ions such as V^{5+} and Cr^{3+} [5, 6], N [7], C [8–10], and S [11–13] ions were decreased. It was important that the optical band edge of the layered anatase thin films did not significantly shift to a longer wavelength region and that they could function as a vis-responsive thin film in the presence of colored materials formed at the interfaces between the layers. These results suggest that anatase thin films with extremely high photoreactivity under UV-light irradiation can be prepared without increasing their specific surface areas.

In order to clarify the factors for designing anatase thin films with higher photoreactivity under UV-light

H. Nagai · M. Hasegawa · H. Hara · C. Mochizuki · M. Sato (✉)
Coordination Engineering Laboratory, Faculty of Engineering, Kogakuin University, 2665-1 Nakano, Hachioji City, Tokyo 192-0015, Japan
e-mail: ft10302@ns.kogakuin.ac.jp

I. Takano
Department of Electronic Engineering, Faculty of Engineering, Kogakuin University, 2665-1 Nakano, Hachioji City, Tokyo 192-0015, Japan

irradiation, we focused on the relationship between the photoreactivity and O-deficiency of anatase thin films fabricated by heat-treatment of precursor films, which were spin-coated on a glass substrate by applying a precursor solution involving the Ti-EDTA complex, in the Ar gas flow.

In this paper, we report the fabrication and characterization of O-deficient anatase thin films with higher photoreactivity under UV-light irradiation; these films were formed by post-annealing thin films formed in an Ar gas flow. The crystal structures and crystallite sizes of the films were characterized by means of XRD. Furthermore, the Raman spectra of the thin films were employed to determine the crystal structure. The chemical identities of the thin films were examined by means of their XPS spectra, and their surface morphologies were observed by means of FE-SEM. Optical characterization of the transparent thin films was carried out by using the absorption spectra and refractive indices. The photoreactivities of the thin films were evaluated on the basis of the pseudo-first-order rate constant of the decoloration of methylene blue dye in an aqueous solution. The formation mechanisms of highly photoreactive anatase thin films and films prepared by using a typical molecular precursor method and a sol–gel procedure in which the heat-treatment of each precursor film was performed in Ar gas flow and air, respectively, were compared.

Experimental

Materials

EDTA, methylene blue (MB), and titanium tetraisopropoxide ($Ti(O^iPr)_4$) were purchased from Kanto Chemical Co., Inc. Dibutylamine and 30% H_2O_2 were purchased from Wako Pure Chemical Industries, Ltd., and from Santoku Chemical Industries Co., Ltd., respectively. Sixty percentage HNO_3 and methanol were purchased from Taisei Chemical Co., Ltd. Ethanol was purchased from Ueno Chemical Industries, Ltd. These solvents were dried on molecular sieves 4 A before use. Other materials were used without further purification. Soda lime glass with a transparent FTO film was purchased from AGC fabritech Co., Ltd. The glass substrate of size 20 × 20 × 1.1 mm^3 for coating was washed in 2-propanol for 15 min by sonicated stirring and then dried in a drying oven at 70 °C.

Preparation of the precursor solution S_{ED} involving the Ti^{4+} complex of EDTA

The precursor solution containing the Ti^{4+} complex of EDTA was obtained by using a method previously reported [14] but slightly modified. To a mixture of 10 g of ethanol and 10 g of methanol, 3.55 g (27.4 mmol) of dibutylamine and 3.65 g (12.4 mmol) of EDTA were added. The solution was refluxed for 2 h by stirring, and then it was cooled to room temperature. After adding 3.55 g (12.4 mmol) of $Ti(O^iPr)_4$, the solution was refluxed for 4.5 h. After cooling the reacted solution to room temperature, 1.56 g (13.7 mmol) of 30% H_2O_2 was carefully added. Subsequently, the solution was refluxed for 0.5 h. The concentration of titanium was 0.4 mmol g^{-1}.

Preparation of the sol–gel solution S_{SG}

A conventional sol–gel solution was prepared by reacting 4.27 g (15.0 mmol) of $Ti(O^iPr)_4$ with 1.09 g (10.3 mmol) of 60% nitric acid and 0.82 g (45.4 mmol) of water in 25 g of ethanol [15, 16]. Thus, the as-prepared solution was obtained. The concentration of titanium was 0.5 mmol g^{-1}.

Coating and heat-treatment procedures and film thickness

Thin films were formed by heat-treatment of the precursor films spin-coated on the FTO glass substrate by applying the solutions S_{ED} and S_{SG} in an Ar gas flow or in air.

The spin-coating method at ambient temperature was used for preparing the precursor films with a double step mode: first at 500 rpm—5 s and then at 2000 rpm—30 s in all the cases. The precursor films were pre-heated in a drying oven at 70 °C for 10 min and then heat-treated at 500 °C for 30 min in an Ar gas flow of 0.1 L min^{-1}. A tubular furnace made of quartz was employed. Thus, the thin films ED and SG obtained by applying the precursor solutions S_{ED} and S_{SG}, respectively, were prepared before annealing in air. Another film ED_{air} was fabricated by firing each precursor film in air at 500 °C for 30 min.

When the concentration of titanium was adjusted to 0.4 mmol g^{-1} for S_{ED}, the film thickness was 100 nm. The sol–gel solution S_{SG} of 0.5 mmol g^{-1} was stirred for 3 days at ambient temperature in order to fabricate the anatase film of thickness 100 nm. The thickness of each film was measured by using a stylus profilometer, DEK-TAK-3 (Sloan).

Post-annealing treatment of the ED, ED_{air}, and SG thin films

The post-annealing treatments of the ED, ED_{air}, and SG thin films were carried out in air at 500 °C for 5, 10, 15, 20, and 30 min. The number in the notation of the post-annealed films indicates the annealing time (min); for example, ED-PA5 indicates that the film ED was post-annealed for 5 min.

Structural characterization of the thin films

The crystal phases of the thin films were examined by using an X-ray diffractometer, MXP-18AHF22 (Bruker AXS), with Cu-$K\alpha$ rays generated using 45 kV and 300 mA. The XRD patterns were measured in the range of 2θ, from 10° to 80° in steps of 0.05° for 2 s. Parallel beam optics with an incident angle of 0.3° was employed for each measurement.

The crystallite size of the anatase crystal formed in each film was measured by using the Scherrer and Hall methods, according to Eq. 1 [17–19], where D, B, λ, η, and θ represent the crystallite size, broadening factor FWHM of the diffraction peak of (101), wavelength of X-ray, random strain, and Bragg angle, respectively. The K value, 0.9, was used as the Scherrer constant. LaB_6 powder (NIST, USA) was employed to obtain the calibration curve.

$$\frac{B\cos\theta}{K\lambda} = \frac{1}{D} + \eta\frac{2\sin\theta}{\lambda} \quad (1)$$

The XRD measurement to determine the crystallite size was performed in the range of 2θ, from 10° to 70° in steps of 0.01° for 10 s.

The Raman spectra of the ED-PA15, ED_{air}-PA15, and SG-PA15 thin films were measured by using a micro-Raman spectrometer, NRS-2000 (JASCO), equipped with a CCD camera and 488-nm incident laser of 1.5 mW. Each spectrum in the wavelength range from 100 to 800 cm^{-1} obtained by exposing the laser beam for 30 s was accumulated 30 times.

The surface appearances of the thin films were observed by using a field-emission scanning electron microscope, FE-SEM S-4200 Hitachi, at an accelerating voltage of 5 kV.

Chemical characterization of the thin films

The thin films were characterized by means of X-ray photoelectron spectroscopy (XPS). A Phi Quantum 2000 Scanning ESCA Microprobe with a focused monochromatic Al-$K\alpha$ X-ray (1486.6 eV) source was employed to evaluate the states and amounts of the elements Ti, O, N, C, and Sn in the thin films. The chemical shift data were charge-referenced to the center of the C–C/C–H peak at 284.6 eV. The resolution was 0.2 eV in each measurement.

The depth profile in the Ar^+ etching mode was obtained by using the same instrument after Ar^+ ion beam bombardment (2 kV and 18 μA cm^{-2}) for 3 min in order to remove surface oxides. The measurements of 15 layers etched stepwise for every 3 min by bombarding Ar^+ ions with the same accelerating energy were performed over an area of 50 μm ϕ of the thin films. In order to examine the O/Ti ratios of the thin film surfaces, XPS spectra of Ti 2p and O 1s peaks were recorded without bombarding Ar^+ ion beams.

Optical characterization of the thin films

The absorption spectra of each thin film were measured in the range from 200 to 800 nm by using a double beam absorption spectrometer, and air was used as a reference in each measurement. The measurements were performed by using a Hitachi U-2800 spectrophotometer.

The optical band edge of each thin film was calculated from the difference spectrum, which was obtained by subtracting the absorption value of the FTO substrate from that of FTO substrate with the thin film at each wavelength. The optical band edge E_g of the thin films was determined by using the following Tauc expression: $\alpha = \frac{A(E-E_g)^{1/2}}{E}$, where E denotes the photon energy ($\equiv h\nu$); A, the constant; and α, the absorption coefficient at wavelength [20].

A MARY-102 (Five Lab) scanning ellipsometer was employed to measure the refractive index of each thin film by using a He–Ne laser beam with a wavelength of 632.8 nm and an incidence angle of 70.8°. The refractive index was measured thrice at eight different spots on the thin films, and each index was determined as the averaged value.

Photoreactivity measurements

The photoreactivity of each thin film of area 15 × 15 mm^2 on the substrate was examined by the decoloration rate of MB in a 10-mL aqueous solution (0.01 mmol L^{-1}). A black light, National FL10BL-B, was used for UV-light irradiation. The distances of the black light sources from the sample surfaces were adjusted to maintain the UV-light intensity at 365 nm as 1.2 mW cm^{-2}, the intensity was measured by using an ultraviolet meter, UVR-400, Iuchi Co., Ltd. The concentration of MB was determined by measuring the absorption spectra of the aqueous solution in the range from 600 to 700 nm by using a Hitachi U-2800 spectrophotometer. At intervals of 20 min during the decoloration test, ca. 3 mL of the solution was transferred into a quartz cell of dimensions 1 × 1 × 4.5 cm^3. After conducting the spectral measurements, the solution was immediately returned to the vessel and mixed with the aliquot. The mixed solution was further used until the test for each film was completed. The temperature of the MB aqueous solution was 20(±1) °C during the measurement. From the absorption spectra at 664 nm of the solutions, each concentration of MB was determined by using a method reported previously [4, 21, 22].

The pseudo-first-order kinetic constant of the decoloration of MB aqueous solutions was obtained thrice for each film, and the averaged value was obtained in terms of the rate constant k. In order to examine the effects of both adsorption and self-decoloration of MB, the same measurement was performed on the same samples without irradiation as a reference.

The k-value for each film was calculated as follows: the concentration of MB after t minutes, C(t), was determined by using formula (I), where Abs(0) and Abs(t) represent the absorption values of the solution immediately before the light irradiation and after t minutes during irradiation, respectively.

$$C(t) = 10 \times \frac{\mathrm{Abs}(t)}{\mathrm{Abs}(0)} \quad (\mu\mathrm{mol\ L^{-1}}) \tag{I}$$

An approximate plot for the function of C(t) versus t was obtained in the range from $0 \leq t \leq 80$ min by using the method of least squares. The rate constant k for each film was estimated as the averaged gradient of the lines by using formula (II), where k_n indicates each gradient obtained thrice ($n = 1, 2, 3$), independently.

$$k = \frac{\Sigma k_n}{3} \times 10^3 \quad (\mathrm{nmol\ L^{-1}\ min^{-1}}) \tag{II}$$

Results

Crystal structures and surface morphologies of the thin films

The XRD patterns of the post-annealed thin films ED-PAn ($n = 5$, 10, 15, 20, and 30 min), along with those of the film ED are shown in Fig. 1. The peaks at $2\theta = 25.3°$ and 53.9° observed for all films are assignable to the (101) and (105) phases of anatase [23]. The peak due to the (200) phase of anatase can be observed at $2\theta = 48.2°$ in the patterns of the post-annealed films ED-PAn ($n \geq 15$). Weak peaks at $2\theta = 27.4°$ observed in the patterns for the post-annealed films ED-PAn ($n \geq 15$) can be assigned to that of the (110) phase of rutile [24]. The peaks at $2\theta = 34.0$, 38.0, 51.9, 62.0, 66.0, and 78.8° in each pattern can be assigned to those of SnO_2 of the FTO substrate [25]. Furthermore, the peaks in the XRD patterns of the films ED_{air} and SG could be assigned to those of anatase and SnO_2 of the FTO substrate. Any additional peak assignable to rutile does not appear in the XRD patterns of the anatase films ED_{air} and SG even after they are post-annealed under the same conditions as those for the film ED.

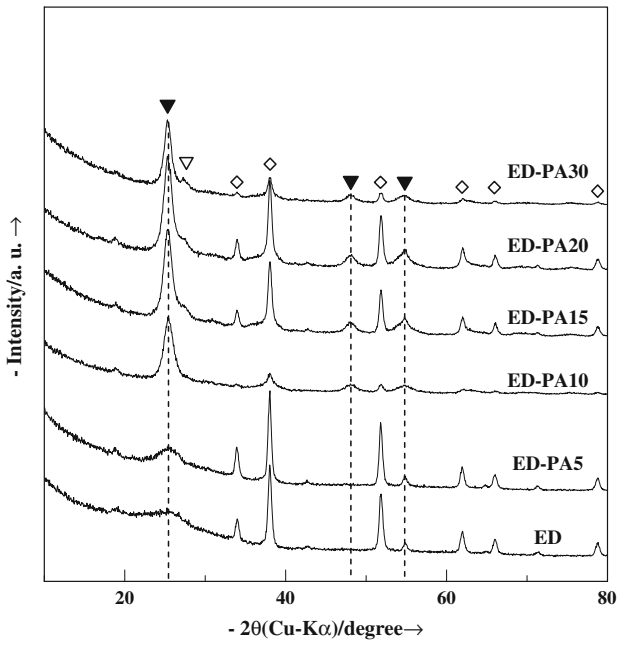

Fig. 1 XRD patterns of ED and ED-PAn thin films, $n = 5$, 10, 15, 20, and 30. The peak assignment is indicated as follows: ▼ Anatase, ▽ Rutile, and ◇ FTO

The crystallite size of each film is presented in Table 1. The thin films ED and ED-PAn have single-nano-size crystallites. The crystallite sizes of the ED_{air} and SG thin films are not significantly affected by the post-annealing treatments.

The Raman spectra of the ED-PA15, ED_{air}-PA15, and SG-PA15 thin films are shown in Fig. 2. The peaks at 144, 399, 519, and 639 cm^{-1} in each pattern are assignable to those of anatase [26].

In Fig. 3, the surface appearances of (A) ED-PA15, (B) ED_{air}-PA15, and (C) SG-PA15 are presented. The surface roughness of both (A) ED-PA15 and (B) ED_{air}-PA15 is ca. 10 nm, which is equal to the resolution of the stylus profilometer used. In comparison with the roughness (100 nm) of the FTO glass substrate, each surface without any crack or pinhole is rather smooth. The surface roughness due to the undulated surface of SG-PA15 having many fine cracks is ca. 25 nm.

Chemical characterization of the thin films by using XPS

Figure 4 shows the XPS spectra of the thin film ED. The binding energy of Ti $2p_{3/2}$ attributed to Ti–O and Ti–N has

Table 1 The crystallite size of anatase in ED, ED_{air}, SG, and post-annealed thin films

Annealing time (min)	ED	ED_{air}	SG
0	–	10	13
5	–	10	13
10	5	11	13
15	4	10	13
20	7	11	13
30	7	12	13

The crystallite size of anatase was measured with a typical Scherrer–Hall method by employing a peak assignable to only (101) of anatase, because other peak intensities due to anatase were too low to measure accurately. The crystallite size of anatase in ED and ED-PA5 could not be obtained because the (101) peak of anatase was also too weak to determine the crystallite size

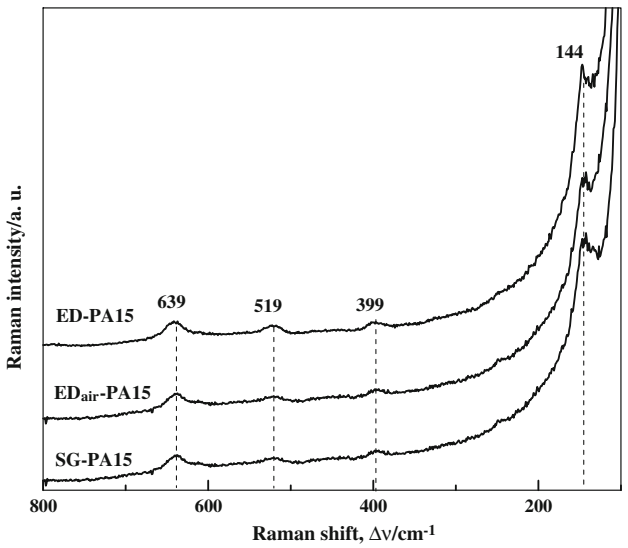

Fig. 2 Raman spectra of ED-PA15, ED_{air}-PA15, and SG-PA15 thin films which were fabricated by post-annealing of ED, ED_{air}, and SG thin films at 500 °C for 15 min in air, respectively

a typical value of 459.2 and 455.8 eV, respectively. The binding energy of O 1*s* with which the O atom bonds to the metal atom is 531.1 eV [27]. The binding energy of N 1*s* is 397.0 eV, and it exists only in the oxygen-substituted form but not in the chemisorption form [28]. These binding energies determined in the thin film ED are identical to those determined in other films fabricated during this study.

The depth profiles measured by using XPS are shown in Fig. 5. Significant amounts of C and N atoms are found, particularly in the thin film (A) ED. These C and N atoms in the thin film ED decrease due to post-annealing treatment, as shown in (B) ED-PA15 and (C) ED-PA30. The amounts of C and N atoms in the thin film (D) ED_{air} are considerably smaller than those in (A) ED. Further, the atoms of C and N atoms found in (D) ED_{air} are decreased by post-annealing treatment, as shown in (E) ED_{air}-PA15 and (F) ED_{air}-PA30. However, neither C nor N atoms are observed in the (G) SG, (H) SG-PA15, and (I) SG-PA30 thin films.

Table 2 shows the averaged O/Ti ratios determined from the XPS peak areas of O 1*s* and Ti $2p_{3/2}$ peaks of the ED, ED_{air}, SG and post-annealed thin films. The averaged values are obtained from each depth profile in the Ar^+ ion etching mode after removing the surface oxides. Extremely small values of the ratio are obtained for the ED and ED_{air} thin films. The values of the SG thin film are not affected by the post-annealing treatment.

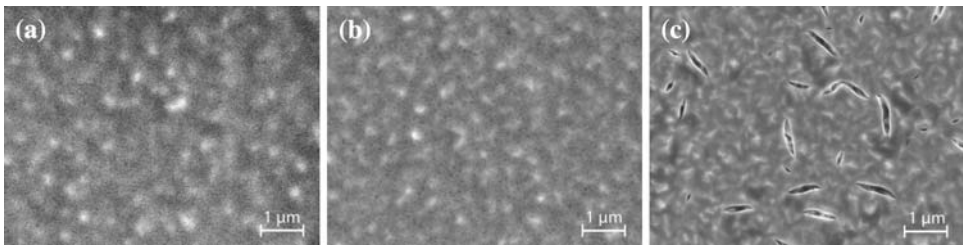

Fig. 3 SEM images of **a** ED-PA15, **b** ED_{air}-PA15, and **c** SG-PA15 thin films obtained by post-annealing the thin films ED, ED_{air}, and SG, respectively, at 500 °C for 15 min in air. Every film thickness is 100 nm

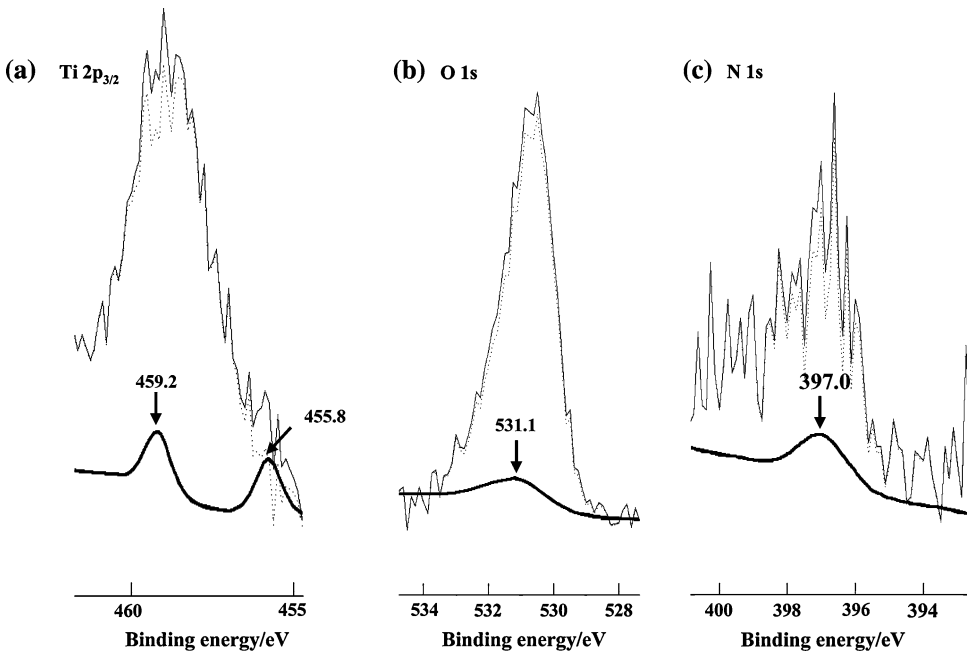

Fig. 4 XPS spectra of **a** Ti $2p_{3/2}$, **b** O 1*s*, **c** N 1*s* of the thin film ED, which was measured after Ar^+ ion beam bombardment (2 kV, 18 μA cm^{-2}) for 3 min for removal of oxides from the surface. The thin *solid lines* indicate the original data of XPS. The thick solid curves are theoretical Gaussian distribution curves. The *dashed curves* show theoretically fitted curves by assuming Gaussian distribution

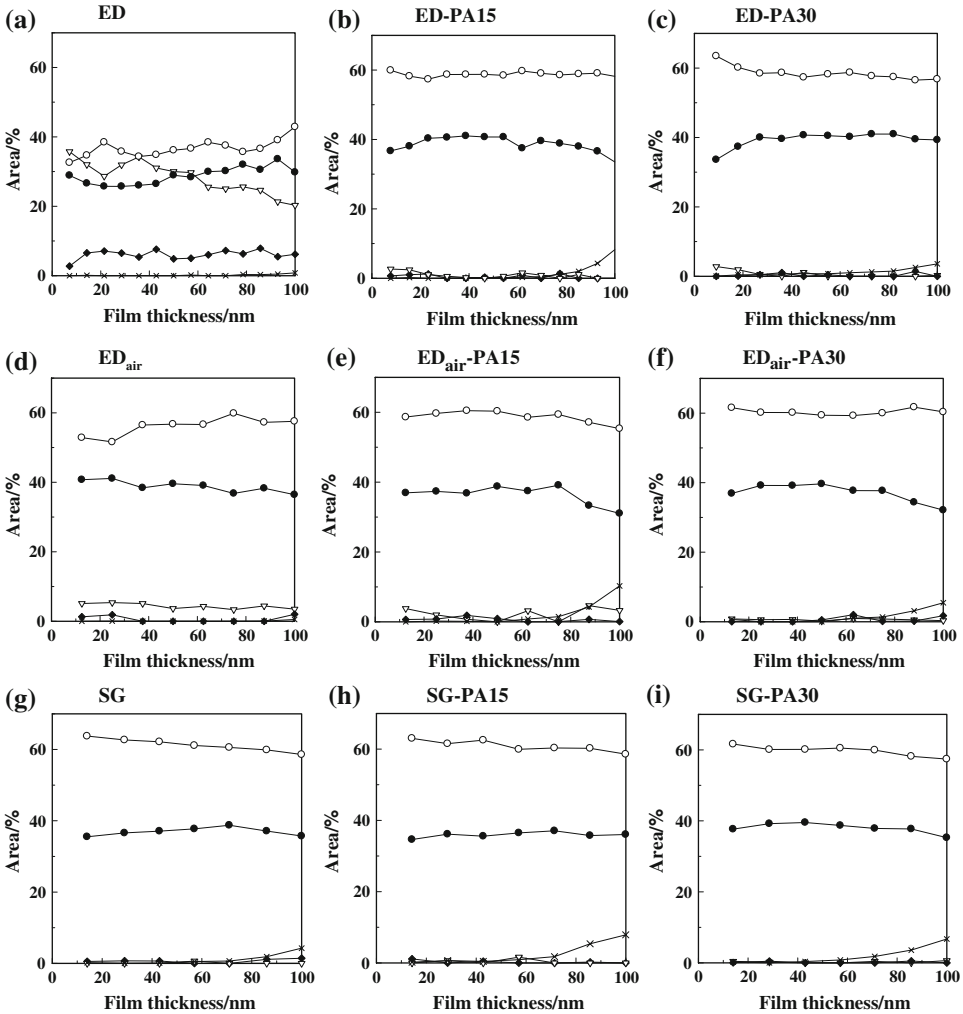

Fig. 5 Depth profile of the elements, Ti, O, N, C, and Sn in the thin films **a** ED, **b** ED-PA15, **c** ED-PA30, **d** ED_{air}, **e** ED_{air}-PA15, **f** ED_{air}-PA30, **g** SG, **h** SG-PA15, and **i** SG-PA30. The energy levels of the five atoms are indicated in parentheses, —●— (Ti 2*p*), —○— (O 1*s*), —◆— (N 1*s*), —▽— (C 1*s*), —×— (Sn 3*d*). Measurement of each 15 layer etched stepwise for every 3 min by bombarding Ar^+ ion with 2 kV and 18 μA cm^{-2} was performed at an area of 50 μm ϕ of the thin films

Table 2 The averaged O/Ti ratios determined by the XPS peak areas of O 1*s* and Ti $2p_{3/2}$ peaks of ED, ED_{air}, SG, and post-annealed thin films

Annealing time (min)	ED	ED_{air}	SG
0	1.37	1.49	1.65
5	1.57	1.61	1.66
10	1.53	1.58	1.66
15	1.49	1.60	1.67
20	1.50	1.60	1.67
30	1.49	1.58	1.68

The XPS peaks of thin films were measured after bombarding Ar^+ ion beam with 2 kV and 18 μA cm^{-2} for 3 min, in order to remove surface oxides. The peak area of O 1 s and Ti 2p was calculated by FWHM and peak height at the positions 531.0 and 459.0 eV, respectively, obtained from each depth profile in Ar^+ ion etching mode

Table 3 The O/Ti ratios determined by the XPS peak areas of O 1*s* and Ti $2p_{3/2}$ peaks observed from the surfaces of ED, ED_{air}, SG, and post-annealed thin films

Annealing time (min)	ED	ED_{air}	SG
0	1.60	1.67	1.92
5	1.61	1.68	1.93
10	1.62	1.68	1.95
15	1.64	1.82	1.96
20	1.72	1.90	1.96
30	1.78	1.96	1.96

The XPS peaks of the thin film surface were measured without bombarding Ar^+ ion beam. The peak area of O 1*s* and Ti 2*p* was calculated by FWHM and peak height at the positions 531.0 and 459.0 eV, respectively

Table 3 shows the O/Ti ratios for thin film surfaces. In comparison with the averaged O/Ti ratios in deep portion (Table 2), these values are considerably large. The O/Ti ratios of the ED and ED_{air} thin film surfaces are remarkably smaller than those of the SG thin film. A gradual increase in the values can be observed when the films are post-annealed.

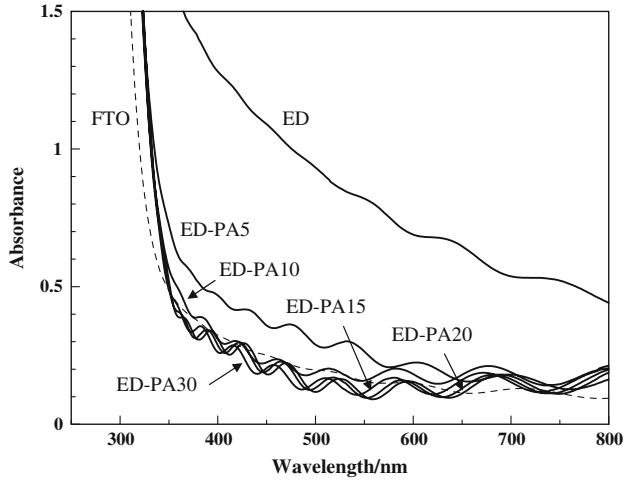

Fig. 6 Absorption spectra of ED and ED-PA*n* thin films whose thickness is 100 nm. The lines indicate each film as follows. ED and ED-PA*n*; ——, FTO substrate; - - - -

Table 4 The optical band edges of ED, ED_{air}, SG and post-annealed thin films

Annealing time (min)	ED	ED_{air}	SG
0	3.43(1)	3.68(1)	3.73(1)
5	3.72(1)	3.74(2)	3.73(1)
10	3.73(2)	3.74(2)	3.72(1)
15	3.74(2)	3.73(2)	3.69(2)
20	3.75(2)	3.73(2)	3.68(1)
30	3.75(1)	3.73(2)	3.66(2)

The edge energy was calculated from the absorption data in the range from 311 to 295 nm of the thin films by employing Tauc expression. Estimated standard deviations are presented in parentheses

Optical characterization of the anatase thin films

The UV–vis absorption spectra of the ED and ED-PA*n* thin films are shown in Fig. 6. It is shown that the absorbance of the films ED and ED-PA5 is remarkably high in the vis-light region, according to the brown color of the film.

The optical band edge shifts of the thin films are listed in Table 4. The band edge shift of the thin film ED is significantly affected by the post-annealing treatment. The optical band edge shift of the thin film SG decreases gradually according to the post-annealing duration, although those of the thin films ED and ED_{air} show a tendency to increase. In comparison with the band edge shift of 3.2 eV for the anatase single crystal, those for thin films are considerably large [29, 30].

Table 5 shows the refractive indices of the thin films. These values lie in the range reported previously for anatase thin films [30, 31]. The refractive indices of the thin films ED_{air} and SG are gradually increased by post-annealing treatment. On the other hand, the refractive index of ED decreases once from 2.17 (ED) to 1.99 (ED-PA15) with the post-annealing treatment, and then it increases with further annealing.

Table 5 The refractive index of ED, ED_{air}, SG, and post-annealed thin films

Annealing time (min)	ED	ED_{air}	SG
0	2.17	2.06	2.06
5	2.07	2.08	2.10
10	2.04	2.08	2.11
15	1.99	2.10	2.11
20	2.00	2.11	2.15
30	2.11	2.13	2.16

The refractive index was measured at eight different spot, and three measurements were performed at each spot

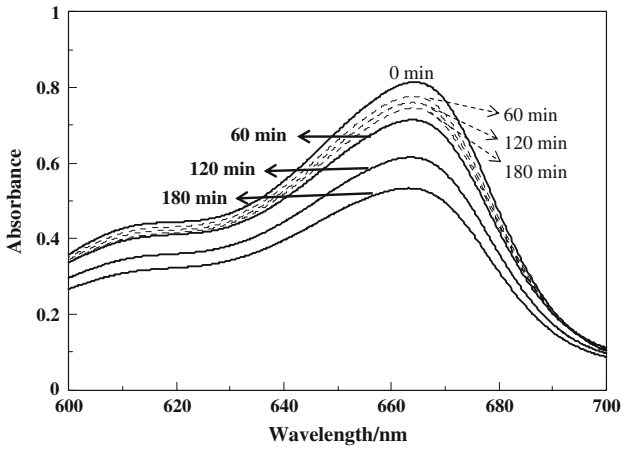

Fig. 7 Spectral changes of MB aqueous solutions during the photoreaction rate measurement by employing ED-PA15 thin film under UV-light irradiation (*solid lines*), along with those under dark (*broken lines*). The absorption value at 664 nm of the solutions was recorded in order to determine the rate constant of the decoloration

Photoreactivity of the anatase thin films

The absorption spectral changes in the MB aqueous solution during decoloration by the film ED-PA15 under UV-light irradiation are shown in Fig. 7, along with those measured under dark conditions. The pseudo-first-order kinetic constant k (nmol L^{-1} min^{-1}) of decoloration of 0.01 mol L^{-1} MB aqueous solution by photoreaction with each thin film under UV-light irradiation is summarized in Table 6, along with that measured for the thin film ED under dark conditions as the reference. The reference values ranging from 3.8 to 4.0 nmol L^{-1} min^{-1} correspond to both adsorption and self-decoloration of MB, and they are independent of the type of thin film.

The k values of the reaction reveal that every film is effective in decolorizing the MB aqueous solution by

Table 6 The pseudo-first-order kinetic constant k (nmol L^{-1} min^{-1}) of decoloration rate of 0.01 mol L^{-1} MB solution by the photoreaction with each thin film under UV-light irradiation

Annealing time (min)	k under UV-light irradiation			k under dark		
	ED	ED_{air}	SG	ED	ED_{air}	SG
0	6.4(1)	9.8(1)	9.1(1)	4.0(1)	4.1(1)	4.0(1)
5	9.1(1)	15.6(1)	10.4(1)	4.0(1)	4.0(1)	4.1(1)
10	12.9(1)	16.3(1)	11.7(1)	3.8(1)	3.9(1)	4.1(1)
15	19.8(3)	13.1(2)	10.5(1)	3.9(1)	3.9(1)	4.0(1)
20	15.0(1)	12.7(1)	11.0(1)	3.8(1)	3.9(1)	3.8(1)
30	12.0(2)	9.1(2)	8.8(1)	3.8(1)	3.8(1)	3.9(1)

The kinetic constant was measured by the decrease of absorption value at 664 nm of each test solution. Those obtained from the data measured under dark are also indicated. Calculated standard deviations are presented in parentheses

photoreaction. The thin film ED-PA15 prepared by post-annealing the ED thin film, which has the lowest photoreactivity, at 500 °C for 15 min in air showed the highest k value. In both cases of ED_{air} and SG thin films, post-annealing treatment for 10 min is mostly effective in enhancing the photoreactivity. However, the effect of post-annealing treatment on the photoreactivities of ED_{air} and SG thin films is unambiguously smaller than that on the thin film ED. In addition, it is notable that the k values of the ED_{air}-PA30 and SG-PA30 thin films are smaller than those obtained before treatment.

In Fig. 8, the photoreactivities of the thin films are presented. Each value is calculated as the difference between the rate constant k under UV-light irradiation and the corresponding value measured for each thin film under dark conditions. As a result, the maximum photoreactivity of ED-PA15 prepared by using the molecular precursor method is 2.1 times higher compared with that of SG-PA10 prepared by the conventional sol–gel procedure.

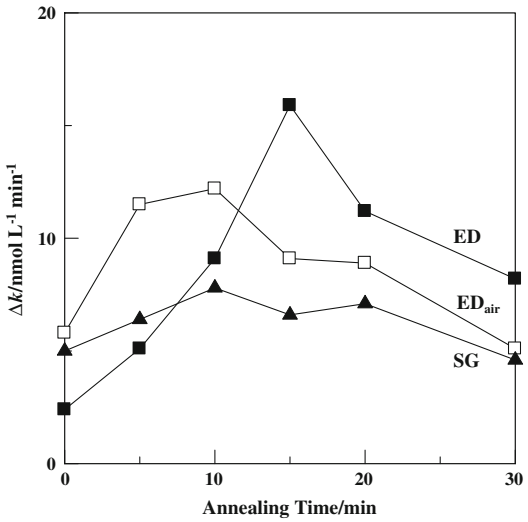

Fig. 8 Dependency of net photoreactivity of each thin film on the post-annealing time. These values were obtained as the differences between the pseudo-first-order kinetic constants (k) of decoloration of MB aqueous solution under UV-light irradiation and those under dark (Table 6). Each line indicates the thin film as follows: ED-PAn; ■—■, ED_{air}-PAn; □—□, SG-PAn; ▲—▲

Discussion

It is generally accepted that the main factors responsible for obtaining anatase with enhanced photoreactivity are (1) high crystallinity, (2) large specific surface area, and (3) low amount of impurity [32, 33]. With regard to these factors, the maximum photoreactivity obtained for the anatase thin film ED-PA15 with higher O-deficiency will be discussed, and then the formation mechanism of the O-deficient anatase by using the molecular precursor method will be discussed.

Crystallinity of the anatase thin films

Crystallite size is an indicator of crystallinity. Among the crystallite sizes of the three anatase thin films ED, ED_{air}, and SG, that of the thin film SG was the largest and that of the film ED was the smallest (Table 1). These sizes of the anatase crystallites in ED_{air} and SG thin films were not affected by post-annealing treatment in air. In contrast, the sizes of the anatase crystallites in the ED thin film were dependent on the annealing time. By means of XPS analyses, it was revealed that the amounts of C and N atoms derived from the EDTA complex in the ED thin film were significantly larger than those in the other thin films. These results suggest that the anatase crystallite in the ED thin film grew effectively with the removal of C and N atoms by annealing the film in air.

Anatase with high crystallinity is generally assumed to have high photoreactivity. However, among the thin films prepared in this study, the thin film ED-PA15, whose crystallite size of anatase is the smallest, indicated the highest photoreactivity in the decoloration of the MB aqueous solution.

Surface morphologies of the anatase thin films

Even surfaces with 10-nm roughness could be observed from the SEM images of the thin films formed by using the molecular precursor method (Fig. 3). Although the specific surface areas of the thin films are not measured quantitatively because of the difficulty involved in the procedure, it can be concluded that the degrees of adsorption of the MB molecule in the aqueous solution are almost equal among the thin films, including those formed by using the sol–gel

method (Table 6). Therefore, the differences between the photoreactivities of these thin films should be attributed to other factors, except the specific surface area.

Purity and optical properties of the anatase thin films

The purity of the transparent thin films was evaluated on the basis of the XPS spectra, and the optical properties were examined on the basis of the absorption spectra and refractive indices of the thin films.

From the XPS spectra (Fig. 5), it is observed that among the thin films, SG and SG-PA*n* show higher purity. Therefore, the highest photoreactivity of the ED-PA15 thin film cannot be attributed to its purity. Doping appropriate amounts of metal ions such as Fe^{3+} and Mg^{2+} into anatase is frequently useful in preventing photo-induced electrons and holes from recombination [34, 35]. However, it is difficult to accept that C and N atoms in ED-PA*n* and ED_{air}-PA*n* contribute toward enhancing their photoreactivities because the UV-light sensitivities of the anatase thin films simply modified by these atoms decrease [7–10]. From this point of view, the purity is not directly related to the highest photoreactivity of ED-PA15.

The strong and wide absorbance in the vis-light region observed in the spectra of the ED and ED-PA5 thin films (Fig. 6) can be attributed to the large amounts of C and N atoms observed in the XPS spectra (Fig. 5), because the absorbance disappears after post-annealing the ED thin film for longer than 10 min.

In comparison with the band edge shift of 3.2 eV for the anatase single crystal, the values of the thin films prepared in this study are larger (Table 4) but comparable with those previously reported for thin films [29, 30]. Because these larger values are mainly attributed to the stress between the thin films and substrates, the stress in the SG thin film can be effectively relaxed by post-annealing. However, it was elucidated that the thin films formed by using the molecular precursor method retain such stresses even after the post-annealing treatment. The ED thin film indicated extremely low values of stress. The result suggests that larger amounts of C and N atoms in the ED thin film produced impurity levels in the band gap, and the gap was drastically affected by eliminating the impurities with the post-annealing treatment for longer than 5 min. A similar but smaller change in the band edge shift in the ED_{air} thin film occurred, because the amounts of C and N atoms in the thin film were considerably smaller than those in ED.

The refractive indices of the thin films (Table 5) lie in the range of values reported for the anatase thin films [30, 31]. The refractive indices of the thin films ED_{air} and SG increased gradually according to the post-annealing duration. On the other hand, the refractive index of the ED thin film decreased once with the post-annealing treatment for 15 min and then increased with further annealing. The largest index, 2.17, of the ED thin film may be attributed to the strong and wide absorbance by the impurities mentioned above. Furthermore, the smallest value, 1.99, of the ED-PA15 thin film could be affected by the largest O-deficiency in the anatase thin film after removal of the impurities. It is suggested that the decrease in permittivity of the thin film was due to the low charge density derived from the O-deficiency, because the structure of anatase is rigidly maintained. The increase in the refractive index by further annealing the thin film may be due to the effects of the addition of oxygen atoms into the lattice (Table 3) and appearance of the rutile phase observed in the XRD spectra (Fig. 1).

Thin film fabrication of O-deficient anatase by using the molecular precursor method

The proposed scheme for O-deficient anatase lattice formation, which can be deduced from the XPS results, is presented in Scheme 1. This scheme indicates a skeleton involving one Ti center in parentheses on the basis that four titanium complexes should be provided to construct at least one unit cell of anatase lattice.

The coordination skeleton of (TiO_4N_2) or (TiO_5N_2) can be assumed in the EDTA complex as a precursor molecule, from the structural study on a Ti complex $[Ti(H_2O)(EDTA)] \cdot 1.5H_2O$ reported by Fackler et al. [36]. In the precursor films, two N and at least four O atoms are linked to one Ti ion.

By heat-treating the precursor complex in the Ar gas flow, neighboring complexes reacted with each other. During the process, several O atoms linked to one Ti ion could be covalently bonded by other Ti ions, and the anatase lattice was gradually structured. By eliminating large amounts of C, H, and N atoms with O atoms, oxide ion sites of the anatase lattice were partially occupied by relatively stable nitride ions derived from the coordinated N atom originally belonging to the ligand. As a result, the total negative charge of the N-substituted anatase in the ED thin film was ca. 3.6, obtained from the summation of 2.8 from the oxide ions and 0.8 from the nitride ions, toward one Ti ion. This charge oriented toward one Ti ion is larger than that, ca. 3.3, due to the oxide ions in the SG thin film (Table 2).

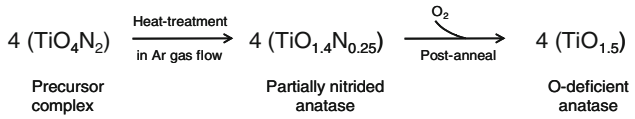

Scheme 1 Proposed scheme for O-deficient anatase lattice formation

The substitutional N atoms could be removed from the anatase lattice by post-annealing the ED thin film. Consequently, the total negative charge of the ED-PA15 thin film whose photoreactivity is highest decreased to ca. 3.0. Annealing treatment for long durations replenished oxide ions into anatase thin films from their surfaces (Table 3), and the photoreactivity was decreased (Fig. 8). Thus, it was elucidated that the O-deficiency is an important factor for controlling the photoreactivity of anatase. It is also notable that the O-deficient anatase lattice is considerably robust, because the stoichiometric Ti_2O_3 did not appear at all.

Conclusion

The molecular precursor method is useful for the fabrication of an O-deficient anatase thin film having higher photoreactivity. The chemical formula of the anatase with the highest photoreactivity under UV-light irradiation can be described as $TiO_{1.5}$, whose O/Ti ratio is quantitatively determined from the XPS spectra. The O-defect sites in anatase of fine crystallites can be generated by post-annealing anatase thin films involving Ti–N bonds derived from the molecular precursor complex. It is notable that the thin film indicates the lowest refractive index.

It was thus revealed that the O-deficiency in anatase thin films is one of the major factors involved in photoreaction by the semiconductor. This factor may be also important to synthesize the anatase powders with high photoreactivity. Therefore, we are now interested in the possibility of rutile thin film fabrication with high photoreactivity by the same principle.

Acknowledgements This study was supported by the "High-Tech Research Center" Project for Private Universities: Matching fund subsidy from Ministry of Education, Culture, Sports, Science and Technology (MEXT) Japan, 2006–2010.

References

1. Fujishima A, Rao TN, Tryk DA (2000) J Photochem Photobiol Chem 1:1. doi:10.1016/S1389-5567(00)00002-2
2. Meshmiri M, Mohseni M, Troczynski T (2004) Appl Catal B 53:209. doi:10.1016/j.apcatb.2004.05.016
3. Yu JC, Yu J, Zhao J (2002) Appl Catal B 36:31. doi:10.1016/S0926-3373(01)00277-6
4. Nagai H, Mochizuki C, Hara H, Takano I, Sato M (2008) Sol Energy Mater Sol Cell 92:1136. doi:10.1016/j.solmat.2008.04.005
5. Anpo M, Kishiguchi S, Ichihashi Y, Takeuchi M, Yamashita H, Ikeue K et al (2001) Che M Res Chem Intermed 27:459. doi:10.1163/156856701104202101
6. Anpo M (2004) Bull Chem Soc Jpn 77:1427. doi:10.1246/bcsj.77.1427
7. Asahi R, Morikawa T, Ohwaki T, Aoki K, Taga Y (2001) Science 293:269. doi:10.1126/science.1061051
8. Irie H, Watanabe Y, Hashimoto K (2003) Chem Lett 32:772. doi:10.1246/cl.2003.772
9. Sakthivel S, Kisch H (2003) Angew Chem Int Ed 42:4908. doi:10.1002/anie.200351577
10. Ohno T, Tsubota T, Toyofuku M, Inaba R (2004) Catal Lett 98:255. doi:10.1007/s10562-004-8689-7
11. Ohno T, Mitsui T, Matsumura M (2003) Chem Lett 32:364. doi:10.1246/cl.2003.364
12. Umebayashi T, Yamaki T, Itoh H, Asai K (2002) Appl Phys Lett 81:454. doi:10.1063/1.1493647
13. Umebayashi T, Yamaki T, Tanaka S, Asai K (2003) Chem Lett 32:330. doi:10.1246/cl.2003.330
14. Sato M, Hara H, Nishide T, Kuritani H, Sawada Y (1996) J Mater Chem 6:1767. doi:10.1039/jm9960601767
15. Brinker CJ, Scherer GW (1990) Sol–gel science. Academic Press, CA, USA
16. Bruce DW, O'Hare D (1992) Inoganic materials. Wiley, Chichester
17. Cullity BD (1978) Elements of X-ray diffraction. Addison-Wesley Publishing Company Inc., USA
18. Sherrer P (1918) Cottingernachr 2:98
19. Hall WH (1950) J Inst Met 75:1127
20. Tanemura S, Miao L, Jin P, Kaneko K, Terai A, Nabatova-Gabain N (2003) Appl Surf Sci 212–213:654. doi:10.1016/S0169-4332(03)00015-1
21. Kwon CH, Shin H, Kim CH, Choi WS, Yoon KH (2004) Mater Chem Phys 86:78. doi:10.1016/j.matchemphys.2004.02.024
22. Ohno T, Tsubota T (2004) Chem Lett 33:750. doi:10.1246/cl.2004.750
23. JCPDS Card 21-1272
24. JCPDS Card 21-1276
25. JCPDS Card 41-1445
26. Ohtsuka T, Guo J, Sato N (1986) J Electrochem Soc 133:2473. doi:10.1149/1.2108452
27. Moses PR, Wier LM, Lennox JC, Finklea HO, Lenhard JR, Murray RW (1978) Anal Chem 50:576. doi:10.1021/ac50026a010
28. Saha NC, Tompkins HG (1992) J Appl Phys 72:3072. doi:10.1063/1.351465
29. Miao L, Jin P, Kaneko K, Terai A, Nabatova-Gabain N, Tanemura S (2003) Appl Surf Sci 212–213:255. doi:10.1016/S0169-4332(03)00106-5
30. Wang Z, Helmerson U, Käll PO (2002) Thin Solid Films 405:50. doi:10.1016/S0040-6090(01)01767-9
31. Nishide T, Sato M, Hara H (2000) J Mater Sci 35:465. doi:10.1023/A:1004731804075
32. Yu JC, Yu J, Zhang L, Ho W (2002) J Photochem Photobiol A 148:263. doi:10.1016/S1010-6030(02)00052-7
33. Kominami H, Kato J, Murakami S, Kera Y, Inoue M, Inui T et al (1999) J Mol Catal Chem 144:165. doi:10.1016/S1381-1169(98)00350-1
34. Bandara J, Kuruppu SS, Pradeep UW (2006) Colloids Surf 276:197. doi:10.1016/j.colsurfa.2005.10.059
35. Xin B, Ren Z, Wang P, Liu J, Jing L, Fu H (2007) Appl Surf Sci 253:4390. doi:10.1016/j.apsusc.2006.09.049
36. Fackler JP Jr, Kristine FJ, Mazany AM, Moyer TJ, Shepherd RE (1985) Inorg Chem 24:1857. doi:10.1021/ic00206a032